ASC Report No. 48/2009

Reconstructing the Knee Joint Mechanism from Kinematic Data

Irene Reichl, Winfried Auzinger, Heinz-Bodo Schmiedmayer, Ewa Weinmüller

Institute for Analysis and Scientific Computing
Vienna University of Technology — TU Wien
www.asc.tuwien.ac.at ISBN 978-3-902627-02-5

Most recent ASC Reports

47/2009 *Irena Rachůnková, Svatoslav Staněk, Ewa Weinmüller, Michael Zenz*
Neumann Problems with Time Singularities

46/2009 *Kazuo Aoki, Ansgar Jüngel, Peter A. Markovich*
Small Velocity and finite Temperature Variations in Kinetic Relaxation Models

45/2009 *Ansgar Jüngel, Jan-Frederik Mennemann*
Time-dependent Simulations of Multidimensional Quantum Waveguides Using a Time-Splitting Spectral method

44/2009 *Markus Aurada, Michael Ebner, Samuel Ferraz-Leite, Petra Goldonits, Michael Karkulik, Markus Mayr, Dirk Praetorius*
HILBERT – A MATLAB Implementation of Adaptive BEM

43/2009 *Matthias Langer, Harald Woracek*
A Local Inverse Spectral Theorem for Hamilton Systems

42/2009 *Ansgar Jüngel*
Energy Transport in Semiconductor Devices

41/2009 *Ansgar Jüngel*
Global Weak Solutions to Compressible Navier-Stokes Equations for Quantum Fluid

40/2009 *Markus Aurada, Petra Goldenits, Dirk Praetorius*
Convergence of Data Perturbed Adaptive Boundary Element Methods

39/2009 *Ilona Gucwa, Peter Szmolyan*
Scaling in Singular Perturbation Problems: Blowing-up a Relaxation Oscillator

38/2009 *Anton Baranov, Harald Woracek*
Majorization in de Branges Spaces III. Division of Blaschke Products

Institute for Analysis and Scientific Computing
Vienna University of Technology
Wiedner Hauptstraße 8–10
1040 Wien, Austria

E-Mail: admin@asc.tuwien.ac.at
WWW: http://www.asc.tuwien.ac.at
FAX: +43-1-58801-10196

ISBN 978-3-902627-02-5

ASC TU WIEN

Mathematical and Computer Modelling of Dynamical Systems
Vol. 00, No. 00, Month 200x, 1–12

RESEARCH ARTICLE

Reconstructing the knee joint mechanism from kinematic data

Irene Reichl[a*], Winfried Auzinger[b], Heinz-Bodo Schmiedmayer[c], and Ewa Weinmüller[b]

[a] *University of Vienna, Institute of Sports Science, A-1150 Vienna, Austria*; [b] *Vienna University of Technology, Institute for Analysis and Scientific Computing, A-1040 Vienna, Austria*; [c] *Vienna University of Technology, Institute of Mechanics and Mechatronics, A-1040 Vienna, Austria*

(*Received 00 Month 200x; final version received 00 Month 200x*)

The interpretation of joint kinematics data in terms of displacements is a product of the type of movement, the measurement technique, and the underlying model of the joint implemented in optimization procedures. Kinematic constraints reducing the number of degrees of freedom are expected to compensate for measurement errors and noise, thus, increasing the reproducibility of joint angles. One approach already successfully applied by several groups approximates the healthy human knee joint as a compound hinge joint with minimal varus/valgus rotation. Most of these optimizations involve an orthogonality constraint. This contribution compares the effect of a model with and without orthogonality constraint on the obtained joint rotation angles. For this purpose kinematic data is simulated without noise and with normally distributed noise of varying size. For small noise the unconstrained model provides more accurate results while for larger noise this is the case for the constrained model. This can be attributed to the shape of the objective function of the unconstrained model near its minimum.

Keywords: tibiofemoral joint; kinematics; optimization; compound hinge joint; model comparison; sensitivity analysis

1. Introduction

The relevance of understanding knee joint kinematics reveals itself in a number of clinical topics. For instance, prostheses have to be designed such that the flexibility and stability characteristics of the human knee joint are reproduced as close as possible in order to limit loosening and accelerated wear. During surgical intervention of lower limb alignment it is also very important to consider joint kinematics.

The interpretation of joint kinematics strongly depends on the measurement process. When using opto-electronic, magnetic or medical imaging techniques markers may be placed invasively or on the skin, the latter involving soft tissue artifacts [1, 2]. Further sources for differing interpretations evolve from the measurement protocol including the marker set and kind of the investigated movement.

An important source for discrepancies between different studies is the fact that the calculated rotation angles strongly depend on the way how the axes locations are defined [3]. For a given definition of the joint rotation axes, the acquisition of anatomical landmarks by palpation is an additional source of error and high intersession variabilities. Thus, functional methods independent of anatomical landmarks are to be preferred, i.e., the kinematic marker data of two adjacent body segments is matched with a kinematical model in order to find the joint rotation axes [4]. In

*Corresponding author. Email: Irene.Reichl@univie.ac.at

ISSN: 1387-3954 print/ISSN 1744-5051 online

DOI: 10.1080/1387395YYxxxxxxxx
http://www.informaworld.com

some cases, e.g., if the range of motion in the concerned joints is too small, functional methods are not applicable. In many clinical applications, the acquisition of full 6 degree of freedom (DOF) knee joint motion data is not required due the reliability of the measurement techniques [5]. A simplified model of the knee joint may lead to a higher reproducibility. It is expected that an appropriate model compensates for measurement errors and reduces effects of noise. However, using a model means that the solution is sought in the subspace defined by the model constraints and further realities could be concealed. The aim of this contribution is to quantify the influence of the kinematical model on the interpretation of measurement data.

2. Current models describing human knee joint kinematics

2.1. *Models using anatomical landmarks*

The human knee is composed of two joints, the patellofemoral and the tibiofemoral joint (TFJ). Here we focus on the TFJ which was intensively studied in the past, involving a paradigmatic shift in the understanding of human knee joint kinematics. Based on observations in the sagittal plane, i.e., in two dimensions, it was concluded that the knee has no fixed flexion/extension (FE) axis. However, the *plane of the FE movement* and the sagittal *observation plane* are tilted by about 5°–10° [6, 7]. Thus, even a fixed axis seems to move as a result of the tilt [8, 9].

Currently, it is widely accepted that within achievable accuracy the FE axis is fixed in the posterior femoral condyles [9]. Observations from active and passive movement are consistent. The assumption of a fixed FE axis is supported by the fact that isometric points on the distal femur - the femoral attachments of the collateral and the cruciate ligaments - can be found [10]. However, there exist several different definitions of the FE axis on the basis of anatomical landmarks. Several authors compare the clinical and the surgical transepiconylar axis, the functional FE axis, and the cylindrical (geometric center) axis [9, 11, 12].

According to [9] TFJ motion can be represented as a pair of independent rotations about two axes. The FE axis is fixed with respect to the femur and the TR axis is fixed in the tibia. Femoral roll back is then the manifestation of tibial (longitudinal) rotation during knee flexion. It was found in [13] that the TR axis was *anterior* to the FE axis (i.e., there is no intersection) and *not* perpendicular to it. The compound hinge theory was tested by estimating the error made as a consequence of the assumption of the two-fixed-axes model [14]. The compound hinge model is supported by observing minor residual displacements, only [7, 15].

The choice of the axes system is substantial. For a mechanical linkage it was demonstrated that an improper selection of the FE and TR axes can result in a virtual screw home motion [16]. Therefore, angles from different studies become comparable first when they are recalculated for the same system of axes.

Additionally, tibial rotation can be influenced by external forces and there is no strict correspondence between extension and tibial rotation [8, 17]. The location of the observed TR axis is task dependent. Therefore, it is necessary to specify the movement task in combination with the recorded joint kinematics.

Further in vitro research identifies two FE axes, one acting in the regime of 150° to 15° of knee flexion and one in the regime until full extension [8, 10].

Summarizing this section it can be stated that the healthy human tibio-femoral joint can be approximated by a model exhibiting two fixed axes [8–11, 13, 15, 18]. For the following investigations, we assume that the TR axis is fixed and the plane of the FE movement is tilted with respect to the sagittal plane [13].

2.2. *Models using kinematic observations and optimization*

An important aim in the biomechanical analysis is the reproducible and user independent description of joint kinematics. With this objective, the positions and orientations of the axes within femur and tibia can be considered as model parameters. By introducing additional constraints like orthogonality and/or intersection of the axes the number of parameters can be reduced. The model parameters can be optimized to 'minimize the difference' of the measured kinematic from the kinematic predicted by the model. It is hypothesized that the optimization procedure will lead to a unique solution with a well defined FE and TR axis. As a result of this procedure the positions and orientations of the FE and TR axes do not depend on anatomical landmarks but are a result of joint kinematics. Surgical interventions such as, e.g., ligament repair or total knee arthroplasty, could profit from interoperative kinematic alignment based on an improved procedure of the joint axes determination.

For the purpose of error compensation, existing optimization procedures take advantage of the fact that under load bearing the finite helical axis (FHA) remains fairly stable between 40° and 80° of flexion [19]. The average FHA in this interval is then defined as the FE axis [20, 21]. The interval 0° to 40° of knee flexion is dominated by flexion and tibial rotation. According to [20], the adduction/abduction and internal/external rotation axis can be selected to form an orthogonal triplet with the FE axis under the constraint of minimizing the adduction/abduction movement in that interval. Another optimization procedure aims at increasing the reproducibility of hip axial rotation angles [22, 23]. In contrast to the former model, not the average FHA, but the line connecting the medial and the lateral femoral epicondyles is defined as the flexion/extension axis. The optimized lower-limb gait analysis (OLGA) technique takes into account not only the kinematic constraints imposed by the knee joint but also those due to the hip and the ankle joint [21]. The functional method proposed in [24] uses the floating axis description by defining the first axis (FE axis) perpendicular to the positions of the tibia during the passive range of movement and the second body fixed axis (TR axis) as the component of the helical axis at 90° of flexion perpendicular to the first axis.

The models described above assume that the FE and the TR axis are coplanar and orthogonal. This is in contrast to the findings of [13] where an *oblique* angle between *non-intersecting* axes is considered, see Sec. 2.1. Although in [14] the authors do not restrict the axes to be coplanar and orthogonal, they fix the direction of the FE and the TR axis due to anatomical landmarks. Therefore, only the location of the TR axis is optimized. In [25], however, intersection of the FE and the TR axis is taken into account and treated as the 'center of the joint'. This represents a 2-degree-of-freedom spherical joint [5].

2.3. *Methods*

2.4. *Kinematic model*

The model used to describe the TFJ consists of intersecting FE axis and TR axis with an oblique angle between them (subfigure 1 (a)). Then the intersection I can be obtained as the joint center by means of coordinate transformation methods or sphere fitting methods. It is further assumed that the direction of the FE axis $\boldsymbol{u}_{FE}$ can be directly calculated in an interval dominated by pure FE-movement and negligible tibial rotation. A modification of the model is also possible by introducing an orthogonality constraint between FE axis and TR axis.

Observing knee joint kinematics is normally done by capturing the relative mo-

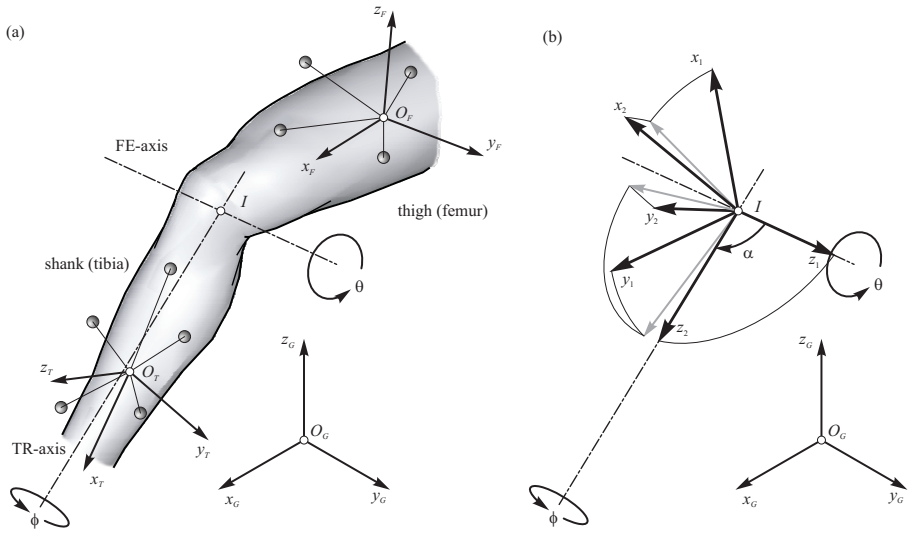

Figure 1. (a) Marker clusters generally moving with respect to global coordinate system $O_G(x_G, y_G, z_G)$ are used to define local coordinate systems (LCS) fixed in the femur $O_F(x_F, y_F, z_F)$ and in the tibia $O_T(x_T, y_T, z_T)$, respectively. In the present model the FE axis and the TR axis intersect at point I but need not to be orthogonal. Angle θ describes the FE-movement whereas ϕ describes the tibial rotation. (b) Two additional LCS are defined. One is fixed in the femur (x_1, y_1, z_1), and the second is fixed in the tibia (x_2, y_2, z_2). The origins of the two LCS coincide with the point I. The z_1-axis lies in the FE axis whereas z_2 coincides with the TR axis. The angle α represents the angle between FE and TR axis.

tion of femur and tibia either using markerless medical imaging techniques (e.g. fast-PC-MRI, X-ray flouroscopy, ...) or marker based methods. In the later case the motion of the bones is recorded either directly by using cortical bone pins or indirectly by using skin mounted markers leading to additional measurement errors (soft tissue artifacts). All of the above techniques allow for the computation of a time dependent local coordinate frame for the thigh (femur) and shank (tibia). Such a time series of two coordinate frames, in general, is the starting point for the calculation of joint axes or centers by means of coordinate transformation and sphere or center fitting methods [26–28]. The *symmetrical axis/center of rotation estimation* (SCoRE) calculates the transformation matrix $R_j(t_i)$ and the vector $\boldsymbol{d}_j(t_i)$, which at time t_i describe the orientation and translation of the segment's coordinate system with respect to a predefined reference orientation and position [27]. Herein $j = 1, 2$ denotes the number of the segment. Although both segments may move arbitrarily with respect to a global frame of reference (global coordinate system GCS) it is assumed that a center of rotation (CoR) or even an axis of rotation (AoR) for the relative movement can be found. Let $\boldsymbol{c}_j$ be the CoR fixed in the LCS of segment j, then the position vector of the CoR in the GCS is given by

$$\boldsymbol{c}_G(t_i) = R_j(t_i)\boldsymbol{c}_j + \boldsymbol{d}_j(t_i)\ ,\ j = 1, 2\ . \tag{1}$$

The estimation of the CoR or AoR is based on the following linear least squares problem,

$$\left(\begin{array}{c|c} R_1(t_1) & -R_2(t_1) \\ \vdots & \vdots \\ R_1(t_N) & -R_2(t_N) \end{array}\right) \left(\begin{array}{c} \boldsymbol{c}_1 \\ \boldsymbol{c}_2 \end{array}\right) = \left(\begin{array}{c} -\boldsymbol{d}_1(t_1) + \boldsymbol{d}_2(t_1) \\ \vdots \\ -\boldsymbol{d}_1(t_N) + \boldsymbol{d}_2(t_N) \end{array}\right)\ . \tag{2}$$

As a consequence of the measurement noise, the global CoR calculated from $\boldsymbol{c}_1$ and $\boldsymbol{c}_2$ do not necessarily coincide, thus, it is suggested to define $\boldsymbol{c}_G$ in the GCS as

the mean between these two positions [27].

It depends on the type of movement and on the joint in question if it is possible to determine a single axis or a center of rotation. In the case of a planar rotation, the matrix of rotation matrices on the left hand side of eqn. 2 has rank five (for exact data). Thus, the result of the minimization has to be an AoR, not a CoR. Measurement noise virtually increases the rank of matrix. A criterion for a planar rotation is that the value of the sixth singular value is small compared to the five others.

For a number of applications, a fixed CoR or AoR may be a poor approximation to describe joint kinematics. Then only an instantaneous axis will be defined. For a joint with pure rotations this axis follows from eqn. 2 solved in a given time slot Δt. In the case of a general displacement including both, translations and rotations, the finite helical axis (FHA) can be calculated. Provided that this is not a pure translation, the two configurations at time t_m and at time t_n are related to each other by a rotation about and a translation along a uniquely defined axis, the FHA.

The ansatz introduced in the present article approximates the healthy knee joint by a compound hinge joint. The optimization procedures assume that the FE axis can be computed in an interval of pure flexion by means of eqn. 2. If the two axes intersect, the center of the joint I is defined as the solution of eqn. 2 within the full range of movement. Since the direction $\mathbf{u}_{FE}$ and the location of the FE axis and the intersection I can be calculated, it is convenient to discuss and solve the problem in a coordinate system where I coincides with the origin and $\mathbf{u}_{FE}$ lies in the z_1-axis (subfigure 1 (b)).

In coordinates of the local femur coordinate system (LCS) the orthogonal tibial basis frame $[E]_{tib|1}(t_n)$ at time t_n reads

$$[E]_{tib|1}(t_n) = R^{fe+tr}(t_n)\,[E]_{tib|1}(t_0)\ . \tag{3}$$

Not only the tibial basis frame obeys eqn. 3, any point fixed with respect to tibia transforms in the same way. The function $R^{fe+tr}(t_n)$ describes the time-dependent relative orientation of the two bodies and will be parameterized as follows,

$$\begin{aligned} R^{fe+tr}(t_n) &= R^{fe}(t_n)\,R^{tr}(t_n)\ , \\ R^{fe}(t_n) &= R_z(\theta(t_n))\ , \\ R^{tr}(t_n) &= Q^{tr}(\alpha,\gamma)\,R_z(\phi(t_n))\,Q^{tr^T}(\alpha,\gamma)\ , \quad Q^{tr}(\alpha,\gamma) = R_z(\gamma)\,R_x(\alpha)\ , \end{aligned} \tag{4}$$

where $R_x(\mu)$ and $R_z(\mu)$ act as a rotation by an angle μ about the x and the z axis, respectively. A rotation about the FE axis simply coincides with a rotation about the z-axis. The direction $\boldsymbol{u}_{TR}$ of the TR axis is is obtained by rotating the vector $(0,0,1)^T$ about the two angles α and γ, see subfigure 1 (b). The unknown parameters are then the time-dependent flexion angle $\theta(t)$, the time-dependent tibial (=internal/external) rotation angle $\phi(t)$, and the two angles α and γ describing the relative location of the TR axis with respect to the FE axis.

In order to reduce the number of unknown parameters, an ansatz for $\theta(t_n)$ and $\phi(t_n)$ has to be implemented. The introduction of such a functional approach has to reflect the reality as close as possible since an unsuitable approach may lead to different kinematic interpretations. Obviously, the shape of the curves for $\theta(t_n)$ and $\phi(t_n)$ depends on the type of movement. The authors therefore suggest to select an initial shape function as a first guess based on the current data. After the parameters have been optimized, new shape functions can be generated to iterate the process of the optimization. The iterative procedure aims at the reduction

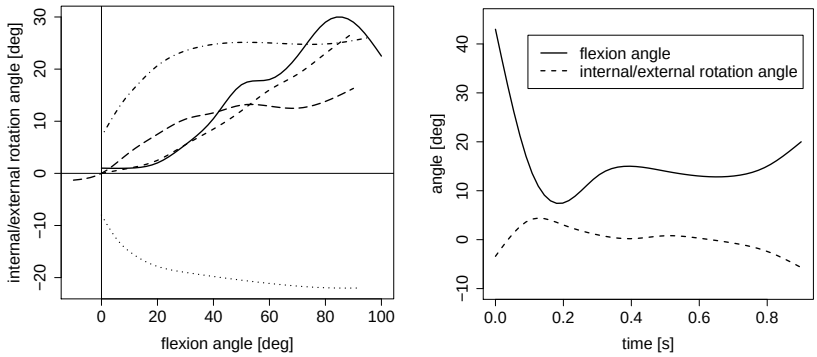

(a) (b)

Figure 2. (a) Passive knee flexion with and without external load. Solid line [29]: constraint based model; short dashed line [29]: reference model; dash-dotted line [30]: external torque of 3Nm; dotted line [30]: internal torque of 3Nm; long dashed line [31]; (b) FE angle and TR angle during a gait cycle [32].
Note that figure (b) shows $\theta(t)$ and $\phi(t)$ while figure (a) plots $\phi(\theta)$. In addition, the range of θ is about 90° in (a) and 35° in (b).

of the manipulative effect of an ansatz function arbitrarily fixed by the observer. Finally, the functions are expected to approach the real shape of $\theta(t_n)$ and $\phi(t_n)$.

In Fig. 2 different shapes of the functions θ and ϕ are compared. Subfigure 2 (a) shows different types of passive knee flexion, with and without external load while subfigure 2 (b) demonstrates gait data. As it can can be seen in Fig. 2, external load stabilizes $\phi(\theta)$ in the range of $\theta \in (40°, 80°)$ [30]. As an input for the optimization procedure a squat movement was also successfully used, see, e.g., [20]. In kinematic data from gait analysis the range of flexion in the stance phase (support phase of body weight) is fairly small.

In our optimization model, the function $\theta(t_n)$ was approximated as a linear function in time. As sample functions for $\phi(\theta)$ the internal/external rotation curves of [30, 31] were approximated by polynomial fits of degree 4. This yields the the initial form of the two functions

$$\theta(t_n) = a_{th}\Big(\frac{t_n}{N}\Big)\ , \quad N = \text{number of time steps} \tag{5}$$

$$\phi(t_n) = a_{ph}\sum_{i=0}^{3} a_i\Big(\frac{t_n}{N}\Big)^i\ . \tag{6}$$

The two angles α and γ representing the orientation of TR with respect to FE and the scaling factors a_{th} and a_{ph} of the time dependent rotation angles $\theta(t)$ and $\phi(t)$ are determined in the optimization procedure. Starting from eqn. 3 the following objective function has to be minimized,

$$\sum_{1\le n\le N} \Big\| [E]_{tib|1}(t_n)[E]^T_{tib|1}(t_0) - R_z(\theta(a_\theta, t_n))\ Q^{tr}(\alpha,\gamma)\ R_z(\phi(a_\phi, t_n))\ Q^{tr^T}(\alpha,\gamma)\ \Big\|^2_F \tag{7}$$

to give the best fit of the model to the given kinematic data set. The index F denotes the Frobenius matrix norm.

For the numerical solution of the resulting minimization problem we use the

function `lsqnonlin` from the MATLAB[1] optimization package. Here, the algorithmic variant based on the Levenberg-Marquardt method has turned out to be most robust and effective. This method is based on an adaptive regularization strategy enforcing monotonous decay of the objective function in each iteration step [33].

The optimized parameter set is then inserted in the time series to calculate an error measure, namely the residual rotation for each step.

2.5. *On the uniqueness of the solution*

Obviously, the solution for $\alpha, \gamma, a_\theta, a_\phi$ is not uniquely defined for only one step from time frame t_l to time frame t_m. Three parameters sufficiently describe this rotation, the rotation axis direction (two angles) and the rotation angle (one angle). By considering at least a second movement step, from time frame t_m to time frame t_n, the solution appears to be unique provided that the movement is not a planar rotation.

To study the behavior of the minimization problem and the performance of the minimization algorithm in more detail, we first consider a model problem with data completely consistent with our model, sampled at 10 observation times. For $\theta(t)$ we choose the quartic polynomial fit according to the model from [31]. We choose $\alpha = \frac{\pi}{2}$, $\gamma = 1.3$, $a_\theta = \frac{\pi}{2}$ and $a_\phi = 0.4494$, and prescribe data exactly fitting our model equations. This means that the prescribed values for α, γ, a_θ and a_ϕ solve the minimization problem, and the residual of the objective function from eqn. 7 vanishes at the solution. As initial guess for the minimization procedure, however, we choose significantly perturbed values for $\alpha, \gamma, a_\theta, a_\phi$, with perturbations of the size of up to 20° and more. MATLAB/`lsqnonlin` returns the true solution up to rounding error, and in all cases tested the convergence behavior was observed to be regular and monotone.

Other algorithmic variants like the classical 'Gauss-Newton method', which is usually more sensitive to the geometry of the objective function, show a significantly more irregular convergence behavior. This may be attributed to the slightly degenerated convexity behavior of the minimization problem: If we fix γ and a_ϕ but let $\alpha \to \alpha + d\alpha$ and $a_\theta \to a_\theta + d\theta$ vary about the true solution, the residual, i.e., evaluation of objective function features a pronounced 'valley' along a curve in the (α, a_θ)-plane passing through the solution. The minimum is indeed unique, but the values of the residual along this curve are significantly smaller than in the region nearby. This situation is visualized in Fig. 3: Here, $d\alpha$ and $d\theta$ are given in degrees, and an appropriately scaled square root of the residual is plotted for the purpose of improved recognizability.

3. Results of the optimization

The optimization parameters in the objective function specified in eqn. 7 are a_θ, α, γ, and a_ϕ. In order to account for the oblique angle between the two fixed hinge axes (model one), the full set of parameters is included into the optimization process. In the model with orthogonality constraint (model two) the angle α between the FE and TR axis is fixed at 90° and only the remaining 3 parameters are optimized. *Residual rotation* is introduced as a measure of the error induced by the above orthogonality constraint. For the time step t_n, the residual rotation is defined as a rotation necessary for the congruency between the tibia frame due to

[1] MATLAB is a trademark of The MathWorks, Inc. Our results are based on release v 7.9 (2009b).

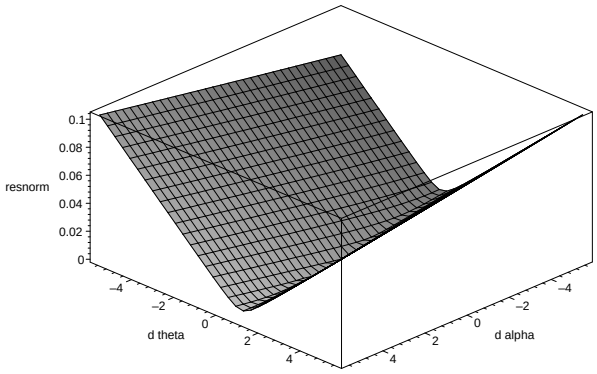

Figure 3. Rescaled values of the residual near the true solution (problem with exact data)

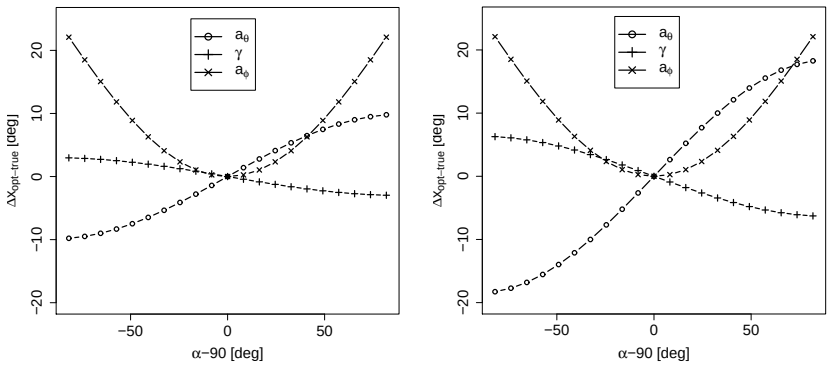

(a) (b)

Figure 4. Differences between the optimized parameters and the true simulation input values for model two with the orthogonality constraint and function $\phi(a_\phi, t_n)$ fitted to data from [19] (a) and [31] (b).

the original data and the tibia frame due to the optimized parameters $(a_\theta, \alpha, \gamma, a_\phi)$ (model one) or $(a_\theta, \alpha = 90°, \gamma, a_\phi)$ (model two). This yields the matrix of residual rotation whose complex eigenvalues are related to the residual rotation angles,

$$[E]_{tib|1}(t_n)[E]^T_{tib|1}(t_0)\left(R_z(\theta(a_\theta, t_n))\, Q^{tr}(\alpha, \gamma)\, R_z(\phi(a_\phi, t_n))\, Q^{tr^T}(\alpha, \gamma)\right)^T . \quad (8)$$

3.1. *Model comparison*

For the numerical simulation, $\theta(a_\theta, t_n)$ and $\phi(a_\phi, t_n)$ are implemented according to eqns. 5 and 6, where $\phi(a_\phi, t_n)$ is fitted to data given in [31] and [19] with a polynomial of degree 4, and γ fixed at 75°.

In the *noise free* case models one and two are compared for α varying in the interval $(0° + \delta, 180° - \delta)$ with $\delta = 8°$. When using model one, true input parameters of the simulation are recovered and consequently, no residual rotations arise. For model two, the optimized parameters $(a_\theta, \gamma, a_\phi)$ deviate from the true values, unless the input parameter $\alpha = 90°$. These deviations are shown in Fig. 4 while in Fig. 5 mean residual rotations are depicted. For $|\alpha - 90°| \leq 20°$ the mean residual rotation does not exceed 3° in both of the model functions for $\phi(a_\phi, t_n)$.

The influence of the *noisy data* is analyzed for $|\alpha_{true} - 90°| \leq 20°$. The data for

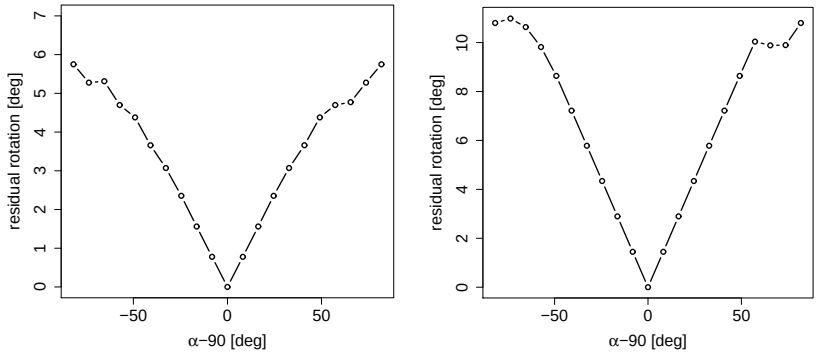

(a) (b)

Figure 5. Residual rotation angles for model two with the orthogonality constraint and $\phi(a_\phi, t_n)$ fitted to data from [19] (a) and [31] (b).

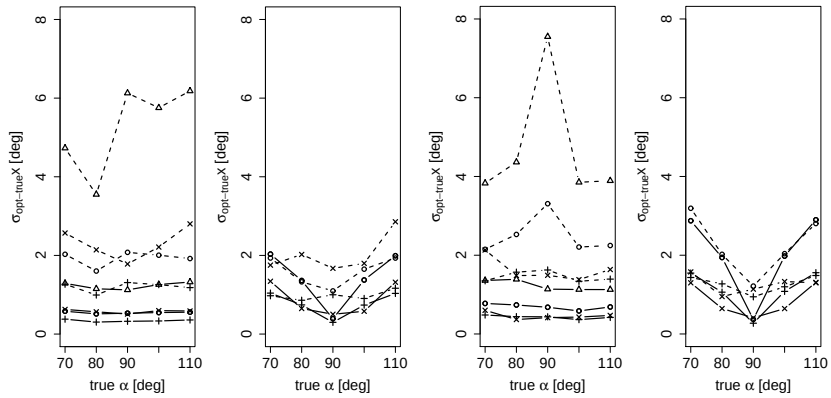

(a) (b)

Figure 6. Noisy data: square root of the mean squared difference $\sigma_{opt-true}$ for the model parameters in the model without (left) and with (right) orthogonality constraint. The standard deviation of the input parameters is $\sigma = 0.29°$ (solid lines) and $\sigma = 2.9°$ (dashed lines); a_θ: circle; α: triangle; γ: cross; a_ϕ: $\times$. Function $\phi(a_\phi, t_n)$ is fitted to data from [19] (a) and [31] (b).

the investigation is provided as before and altered by adding a normally distributed error (using routine `randn` from MATLAB) to all of the four parameters. Test runs are performed for $\sigma = 2.9°$ and $\sigma = 0.29°$. For the same set of values for σ and α, the data simulation and parameter optimization are repeated 20 times. Fig. 6 shows the square root of the mean squared difference $\sigma_{opt-true}$ of optimized and true parameters. For both model functions $\phi(a_\phi, t_n)$, the application of model one results in a large deviation in the calculated value of α. This can be attributed to the behavior of the objective function near its minimum, see Sec. 2.5. The minimum in α is not sharply pronounced. The residual rotation angles for models one and two and for both functions $\phi(a_\phi, t_n)$ are comparably small, see Fig. 7.

4. Discussion and outlook

In this article, the compound hinge joint with intersecting axes was tested for a model with and without orthogonality constraint. The experiments indicate that

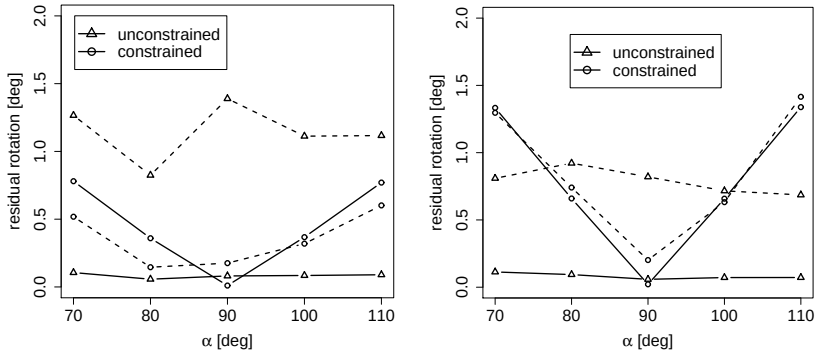

(a) (b)

Figure 7. Mean residual rotation angles for the model with and without orthogonality constraint. The standard deviation of the input parameters was $\sigma = 0.29°$ (solid lines) and $\sigma = 2.9°$ (dashed lines). Function $\phi(a_\phi, t_n)$ is fitted to data from [19] (a) and [31] (b).

for the case of a joint with an oblique angle between the FE and TR axis, the unconstrained model matches the data closer than the constrained model. It turns out that for the unconstrained model and the exact data, the error of the numerical approximation for the model parameters stays in the range of the round-off errors. However, in contrast to naive expectations, it is also fairly small for the constrained model. Taking measurement noise into account considerably reduces the differences in both models in context of the achieved accuracy of the model parameters. This can be explained by the fact that the minimum of the objective function is not sharply pronounced in α, as it is shown for exact data in Sec. 2.5. Due to the sharp 'valley' along a curve in the (α, a_θ)-plane, the minimum cannot be found easily. For noisy data the objective function is deformed and therefore, finding its minimum becomes more difficult.

The behavior of the objective function described above is based on a small set of numerical experiments. However, it seems to be typical and can also be observed for other data configurations. However, since the Levenberg-Marquardt method performs successfully, this seems to indicate a potential direction of refinement. For our model, admissible values for α and a_θ appear to be correlated. This suggests that restricting the range of admissible values by modelling this correlation in an appropriate way – alternatively to a common model with a fixed orthogonality constraint – may lead to more reliable results in practical applications.

We also note that for all other numerical tests based on the present model, as well as a model with orthogonality constraint, presented in Sec. 3, the performance of `lsqnonlin` with activated algorithmic option 'Levenberg-Marquardt' was working completely satisfactory, and no convergence problems were reported by the code.

In this contribution two models describing human knee joint and their sensitivity with respect to noise were tested using sets of simulated data. We plan to continue this study and apply the presented approach to the real-world data. In this case, the shape functions for $\theta(a_\theta, t_n)$ and $\phi(a_\phi, t_n)$ have to be interpreted as starting guesses for the unknown true functions. After the optimization of parameters $\alpha, \gamma, a_\theta, a_\phi$ new shape functions are generated. Since this optimization procedure can be iterated, the question concerning its convergence arises.

It was mentioned in Sec. 2 that the knee axes do not intersect. This feature shall

be confirmed for the realistic data. Furthermore, another interesting question shall be addressed - can the computational algorithm find a second FE axis in the range until full extension [8, 10].

Acknowledgments

This work was supported by the FWF (Austrian Science Fund), contract number T318-N14.

List of abbreviations

ACL	anterior cruciate ligament
AoR	axis of rotation
DOF	degrees of freedom
FE	flexion-extension
FHA	finite helical axis
OLGA	optimized lower-limb gait analysis
TFJ	tibiofemoral joint
TR	tibial-rotation

References

[1] S.J. Piazza, N. Okita, and P.R. Cavanagh, *Accuracy of the functional method of hip joint center location: effects of limited motion and varied implementation*, Journal of Biomechanics 34 (2001), pp. 967–973.

[2] V. Camomilla, A. Cereatti, G. Vannozzi, and A. Cappozzo, *An optimized protocol for hip joint centre determination using the functional method*, Journal of Biomechanics 39 (2006), pp. 1096–1106.

[3] H. Woltring, *3-D attitude representation of human joints: A standardization proposal*, Journal of Biomechanics 27 (1994), pp. 1399–1414.

[4] S. Martelli, S. Zaffagnini, B. Falcioni, and M. Marcacci, *Intraoperative kinematic protocol for knee joint evaluation*, Computer Methods in Biomechanics and Biomedical Engineering 62 (2000), pp. 77–86.

[5] A.M. Bull and A.A. Amis, *Knee joint motion: description and measurement*, Proceedings of the I Mech E Part H. Journal of Engineering in Medicine 212 (1998), pp. 357–372.

[6] R. Fick *Handbuch der Anatomie und Mechanik der Gelenke.*, Vol. 2, Verlag Gustav von Fischer, Jena, 1911.

[7] D.L. Churchill, S.J. Incavo, C.C. Johnson, and B.D. Beynnon, *The transepicondylar axis approximates the optimal flexion axis of the knee*, Clin Orthop (1998), pp. 111–118.

[8] P.N. Smith, K.M. Refshauge, and J.M. Scarvell, *Development of the concepts of knee kinematics.*, Arch Phys Med Rehabil 84 (2003), pp. 1895–1902.

[9] T. Asano, M. Akagi, and T. Nakamura, *The Functional Flexion-Extension Axis of the Knee Corresponds to the Surgical Epicondylar Axis: In Vivo Analysis Using a Biplanar Image-Matching Technique.*, The Journal of Arthroplasty 20 (2005), pp. 1060–1067.

[10] S.G. Elias, M.A. Freeman, and E.I. Gokcay, *A correlative study of the geometry and anatomy of the distal femur*, Clin Orthop (1990), pp. 98–103.

[11] E. Most, J. Axe, H. Rubash, and G. Li, *Sensitivity of the knee joint kinematics calculation to selection of flexion axes.*, Journal of Biomechanics 37 (2004), pp. 1743–1748.

[12] D.G. Eckhoff, J.M. Bach, V.M. Spitzer, K.D. Reinig, T.F. Dwyer, M.M. Bagur, T.H. Baldini, D. Rubinstein, and S. Humphries, *Three-Dimensional Morphology and Kinematics of the Distal Part of the Femur Viewed in Virtual Reality*, Journal of Bone and Joint Surgery 85-A Suppl 4 (2003), pp. 97–104.

[13] A.M. Hollister, S. Jatana, A.K. Sing, W.W. Sullivan, and A.G. Lupichuk, *The Axes of Rotation of the Knee*, Clinical Orthopaedics and Related Research 290 (1993), pp. 259–268.

[14] D.L. Churchill, S.J. Incavo, C.C. Johnson, and B.D. Beynnon, *A compound pinned hinge model of knee joint kinematics*, Trans. Orthop. Res. Soc. 42 (1996), p. 717.

[15] ———, *A novel method for quantifying knee joint kinematics: the compound pinned hinge model*, Twenty-First Annual Meeting of the American Society of Biomechanics Clemson University, South Carolina, September 24-27 (1997).

[16] S.J. Piazza and P.R. Cavanagh, *Measurement of the screw-home motion of the knee is sensitive to errors in axis alignment*, Journal of Biomechanics 33 (2000), pp. 1029–1034.

[17] A.S. Levens, V.T. Inman, and J.A. Blosser, *Transverse rotations of the segments of the lower extremity in locomotion*, Journal of Bone and Joint Surgery 30A (1948), pp. 859–872.

[18] D.G. Eckhoff, T.F. Dwyer, J.M. Bach, V.M. Spitzer, and K.D. Reinig, *Three-dimensional morphology of the distal part of the femur viewed in virtual reality*, Journal of Bone and Joint Surgery American Volume 83-A Suppl 2 (Pt 1) (2001), pp. 43–50.

[19] L. Blankevoort, R. Huiskes, and A. Langede , *Helical axes of passive knee joint motions*, Journal of Biomechanics 23 (1990), pp. 1219–1229.

[20] F. Marin, H. Mannel, L. Claes, and L. Dürselen, *Correction of axis misalignment in the analysis of knee rotations*, Human Movement Science 22 (2003), pp. 285–296.

[21] I.W. Charlton, P. Tate, P. Smyth, and L. Roren, *Repeatability of an optimised lower body model*, Gait & Posture 20 (2004), pp. 213–221.

[22] R. Baker, L. Finney, and J. Orr, *A new approach to determine the hip rotation profile from clinical gait analysis data*, Human Movement Science 18 (1999), pp. 655–667.

[23] A.G. Schache, R. Baker, and L.W. Lamoreux, *Defining the knee joint flexion-extension axis for purposes of quantitative gait analysis: An evaluation of methods*, Gait & Posture 24 (2006), pp. 100–109.

[24] S. Martelli, S. Zaffagnini, B. Falcioni, and M. Motta, *Comparison of Three Kinematic Analyses of the Knee: Determination of Intrinsic Features and Applicability to Intraoperative Procedures*, Computer Methods in Biomechanics and Biomedical Engineering 5 (2002), pp. 175–185.

[25] R. Ward, R. Baker, and A. Schache, *Anatomical constraints of the lower limb joints: Implications for kinematic modelling for quantitative gait analysis*, Gait & Posture 24 (2006), pp. S103–S104.

[26] M.H. Schwartz and A. Rozumalski, *A new method for estimating joint parameters from motion data*, Journal of Biomechanics 38 (2005), pp. 107–116.

[27] R.M. Ehrig, W.R. Taylor, G.N. Duda, and M.O. Heller, *A survey of formal methods for determining the centre of rotation of ball joints*, Journal of Biomechanics 39 (2006), pp. 2798–2809.

[28] ———, *A survey of formal methods for determining functional joint axes*, Journal of Biomechanics 40 (2007), pp. 2150–2157.

[29] N. Akalan, M. Özkan, and Y. Temelli, *Three-dimensional knee model: Constrained by isometric ligament bundles and experimentally obtained tibio-femoral contacts*, Journal of Biomechanics 41 (2008), pp. 890–896.

[30] L. Blankevoort and R. Huiskes, *Validation of a three-dimensional model of the knee*, Journal of Biomechanics 29 (1996), pp. 955–961.

[31] K.E. Moglo and A. Shirazi-Adl, *Cruciate coupling and screw-home mechanism in passive knee joint during extensionflexion*, Journal of Biomechanics 38 (2005), pp. 1075–1083.

[32] M.S. Andersen, D. Benoit, M. Damsgaard, D. Ramsey, and J. Rasmussen, *Do kinematic models reduce the effects of soft tissue artefacts in skinmarker- based motion analysis? An in vivo study of knee kinematics*, Journal of Biomechanics (2009).

[33] J.J. Moré, *The Levenberg-Marquardt algorithm: Implementation and theory*, Lecture Notes in Mathematics 630 (1977), pp. 105–116.